

Dalton Transactions

Accepted Manuscript



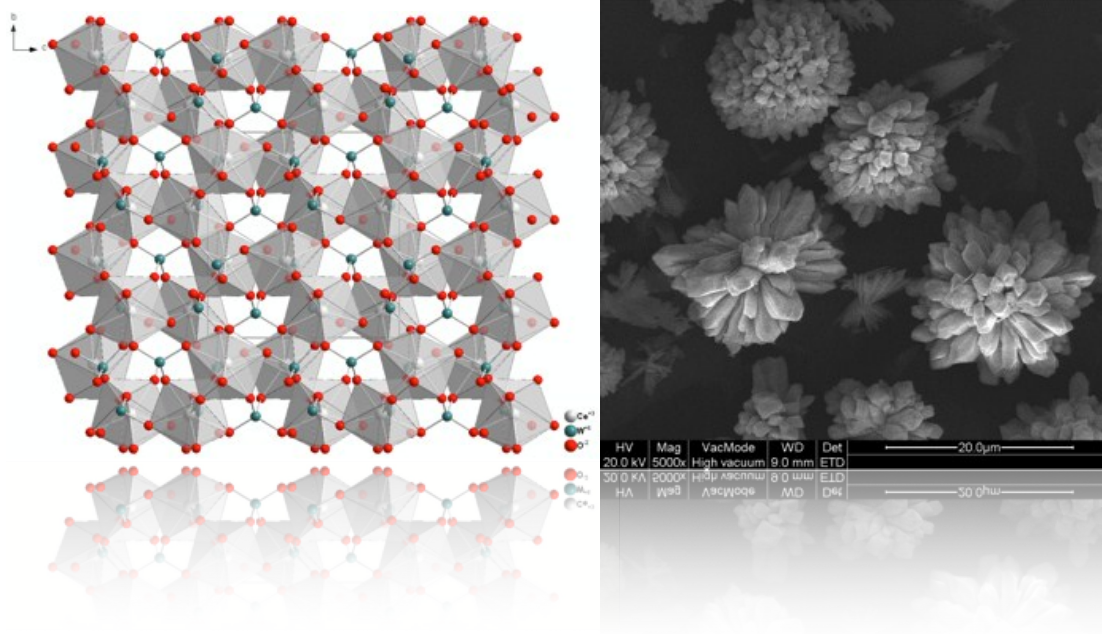
This is an *Accepted Manuscript*, which has been through the Royal Society of Chemistry peer review process and has been accepted for publication.

Accepted Manuscripts are published online shortly after acceptance, before technical editing, formatting and proof reading. Using this free service, authors can make their results available to the community, in citable form, before we publish the edited article. We will replace this *Accepted Manuscript* with the edited and formatted *Advance Article* as soon as it is available.

You can find more information about *Accepted Manuscripts* in the [Information for Authors](#).

Please note that technical editing may introduce minor changes to the text and/or graphics, which may alter content. The journal's standard [Terms & Conditions](#) and the [Ethical guidelines](#) still apply. In no event shall the Royal Society of Chemistry be held responsible for any errors or omissions in this *Accepted Manuscript* or any consequences arising from the use of any information it contains.

Various $\text{Ce}_2(\text{WO}_4)_3$ and $\text{Ce}_{10}\text{W}_{22}\text{O}_{81}$ 3D microstructures prepared hydrothermally in the absence and presence of a surfactant are reported. The different luminescence properties of the two types of materials, when doped with Tb^{3+} ions were investigated and appropriate energy transfer mechanisms are suggested.



Cite this: DOI: 10.1039/c0xx00000x

www.rsc.org/xxxxxx

ARTICLE TYPE

Green and blue emitting 3D structured Tb: Ce₂(WO₄)₃ and Tb: Ce₁₀W₂₂O₈₁ micromaterials

Anna M. Kaczmarek,*^a Dorine Ndagsi,^a Isabel Van Driessche,^c Kristof Van Hecke,^b Rik Van Deun*^a*Received (in XXX, XXX) Xth XXXXXXXXXX 20XX, Accepted Xth XXXXXXXXXX 20XX*

DOI: 10.1039/b000000x

In this paper, various microstructures of Ce₂(WO₄)₃ and Ce₁₀W₂₂O₈₁ were prepared by applying a hydrothermal synthesis, in a ligand-free environment, and in the presence of dioctyl sodium sulfosuccinate (DSS) surfactant, after which the materials were heat treated at a temperature of 900 °C. Depending on the concentration of cerium ions to sodium tungstate, as well as the reaction pH, two different cerium tungstate materials were obtained. The source of cerium, and the presence or absence of the surfactant had a significant influence on the morphology of the final product. The photoluminescence properties of Tb³⁺ doped cerium tungstate materials were investigated. Luminescence measurements showed an efficient charge transfer from the tungstate groups to the Tb³⁺ ions. All the materials emitted blue or green light under UV excitation.

15 Introduction

For years now the synthesis of inorganic materials with controlled morphology has been a tremendously important and interesting research topic. The large interest in the subject originates from the observation that a strong correlation exists between the size, shape, and morphology of particles and their properties.¹⁻² Additionally it is known that particle aggregates can have collective properties different from the properties of individual particles as well as of the bulk material. This gave rise to an interest in fabricating 3D structured materials built from nano- and micro- building blocks. In lanthanide doped materials the modification of a material's size can cause changes in its luminescence properties e.g. different peak positions, intensities and splitting in the emission spectra, as well as changes in the luminescence lifetimes, quantum efficiencies, and concentration quenching.³⁻⁵ Most of these changes can be linked to the structure distortions and surface defects caused by the size reduction – these structure distortions and surface defects affect the local environment of the lanthanide ion giving rise to different symmetry, crystal field strength, and index of refraction compared to the bulk material.

Materials doped with lanthanide ions possess fascinating optical properties and have found various applications, especially in the lighting industry.⁶ Rare-earth tungstate nano- and micro- sized materials are interesting materials due to their possible applications, especially in the field of luminescence when doped with trivalent lanthanide ions. Previous reports on rare-earth tungstates prove that they can be very good host lattices for the luminescence of lanthanide ions.⁷⁻⁹ When the material is excited into the tungstate groups energy may be effectively transferred to the doped lanthanide ions. If the transfer of energy from the tungstate groups to the lanthanide ions is not complete the

tungstate groups emit blue-green light themselves. Lanthanum and yttrium tungstate compounds are suitable hosts, because lanthanum has no f electrons and yttrium is a spectroscopically silent ion, and unless other light emitting components are present, no f-f transitions are possible. This is not the case with cerium compounds, which emit a broad band in the blue-green region. Tungstate materials at the nano-/micro- size have been obtained using a variety of synthetic techniques such as the hydrothermal method (which is the most often employed synthetic technique for these materials), microwave-assisted hydrothermal method, molten salt synthesis, sol-gel synthesis, and others. Factors such as the presence of a ligand, reaction time and temperature, reaction pH, and source of rare-earth and tungstate ions were found to be most important in attempts to obtain materials with specific morphologies. This research was thoroughly outlined by two of us in a recent review on rare-earth tungstate and molybdate materials.¹⁰ Despite the quite large amount of reported rare-earth tungstate materials (for example Y₂WO₆, Gd₂(WO₄)₃, Y₂(WO₄)₃, NaY(WO₄)₂, AgLa(WO₄)₂), to the best of our knowledge 3D structured Ce₂(WO₄)₃ have not been reported before.¹¹⁻¹⁵ Up until now only nanosized Ce₂(WO₄)₃ particles, obtained in a reversed microemulsion synthesis, have been reported by Pramanik et al.¹⁶ A Ce₁₀W₂₂O₈₁ nano- or micro- sized material has not been reported so far.

This research was undertaken with two motivations. First, it was intended to synthesize 3D structured Ce₂(WO₄)₃ and Ce₁₀W₂₂O₈₁ materials, built from nano- or micro- sized building blocks. By varying reaction conditions, such as the source of lanthanide ions and the presence of a structure directing agent – dioctyl sodium sulfosuccinate (DSS), four Ce₂(WO₄)₃ materials with different 3D architectures were obtained. By changing the pH value from 8-9 to pH 7, and the concentration of cerium to tungstate, a

$\text{Ce}_{10}\text{W}_{22}\text{O}_{81}$ material was obtained (only when $\text{Ce}(\text{NO}_3)_3$ was used as the source of cerium ions). The second motivation was to dope Tb^{3+} ions into the cerium tungstate matrixes and investigate the luminescence properties of the material. Tb^{3+} ions were chosen because it is known that it is feasible to excite Tb^{3+} ions by energy-transfer from Ce^{3+} ions (indirect excitation).

Experimental Section

All chemicals (analytical grade) were purchased from Sigma Aldrich and used without further purification.

10 Synthesis of $\text{Tb}^{3+}:\text{Ce}_2(\text{WO}_4)_3$ (samples 1-4)

Samples were synthesized hydrothermally in the presence and absence of DSS surfactant. When DSS was used first 1 mmol of DSS was dissolved in 20 mL distilled water. 1 mmol of $\text{RE}(\text{NO}_3)_3$ or $\text{RE}(\text{OAc})_3$ ($\text{RE} = \text{Ce}^{3+}, \text{Tb}^{3+}$) salts at the right percentage amounts were weighed off and dissolved together in 15 10 mL of water. The dissolved salts were slowly added to the DSS solution while stirring on a magnetic stirrer. After 10 minutes 1.5 mmol Na_2WO_4 dissolved in 10 mL water was slowly added. The pH of the solution was left without adjusting. After 10 minutes the suspension was transferred into an autoclave and heated at 200 °C for 24h (at an oven heating rate of 1 °C per minute). After the end of the heating time the autoclave was cooled naturally to room temperature, the precipitate centrifugated, and the product washed two times with water and 25 two times with methanol. The product was dried in a vacuum oven at 60 °C. To obtain the final product the precursor material (as prepared product) was heat treated in air at 900 °C for 3h.

Synthesis of $\text{Tb}^{3+}:\text{Ce}_{10}\text{W}_{22}\text{O}_{81}$ (samples 5-6)

Samples were synthesized hydrothermally in the presence and absence of DSS surfactant. When DSS was used first 1 mmol of DSS was dissolved in 20 mL distilled water. 1 mmol of $\text{RE}(\text{NO}_3)_3$ or $\text{RE}(\text{OAc})_3$ ($\text{RE} = \text{Ce}^{3+}, \text{Tb}^{3+}$) salts at the right percentage amounts were weighed off and dissolved together in 10 mL of water. The dissolved salts were slowly added to the 35 DSS solution while stirring on a magnetic stirrer. After 10 minutes 1 mmol Na_2WO_4 dissolved in 10 mL water was slowly added. The pH of the solution was adjusted to pH 7 by adding a few drops of diluted HNO_3 . After 10 minutes the suspension was transferred into an autoclave and heated at 200 °C for 24h (at an oven heating rate of 1 °C per minute). After the end of the heating time the autoclave was cooled naturally to room temperature, the precipitate centrifugated, and the product washed two times with water and two times with methanol. The product was dried in a vacuum oven at 60 °C. To obtain the final product the precursor material (as prepared product) was heat treated in air at 900 °C for 3h.

Characterization

SEM measurements were performed using a FEI Quanta 200 FSEM and an FEI Nova 600 Nanolab Dual-Beam focused ion beam in secondary electron mode. XRD patterns were recorded by a Thermo Scientific ARL X'TRA diffractometer equipped with a $\text{Cu K}\alpha$ ($\lambda = 1.5405 \text{ \AA}$) source, a goniometer and a Peltier cooled $\text{Si}(\text{Li})$ solid state detector. Chemical bonding was analyzed by infrared spectroscopy, using a Thermo Scientific

55 FTIR spectrometer (type Nicolet 6700) equipped with a DRIFTS-cell. Samples were prepared by mixing the powders with KBr. The samples were measured in the 550-4000 cm^{-1} range. The luminescence of solid samples was studied. Solid powdered samples were put between quartz plates (Starna cuvettes for 60 powdered samples, type 20/C/Q/0.2). Luminescence measurements were done on an Edinburgh Instruments FLSP920 UV-vis-NIR spectrometer setup. A 450W xenon lamp was used as the steady state excitation source. A Hamamatsu R928P photomultiplier tube was used to detect the emission signals in the near UV to visible range. All of the luminescence measurements were recorded at room temperature. In order to compare the measurements the same amounts of powders were used as well as the same settings for each measurement (same slit size, step, and dwell time). The excitation spectra included in the 70 manuscript have not been corrected for detector sensitivity. All emission spectra in the manuscript have been corrected for detector sensitivity. The CIE color coordinates were calculated using ColorCalculator 4.97 freeware program provided by Osram Sylvania.

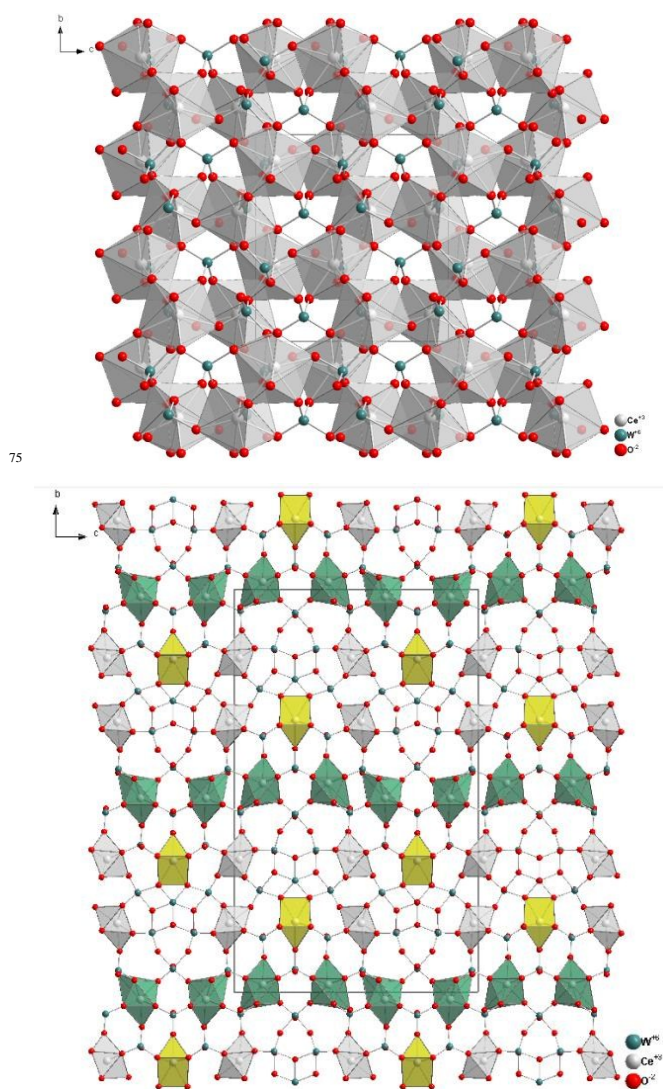


Fig. 1 Top: crystal structure of $\text{Ce}_2(\text{WO}_4)_3$. Bottom: crystal structure of $\text{Ce}_{10}\text{W}_{22}\text{O}_{81}$

Results and discussion

Structure and morphology

Table 1. Brief summary of reaction conditions, corresponding product morphologies, and assigned symbols, which will be used throughout the paper.

Sample	Ln source	DSS [mmol]	Reaction pH	Morphology of product
1	Ce(NO ₃) ₃	0	8-9	Irregular flower-like microspheres around 2 – 3 μm in diameter assembled from nanorods (nanoparticles additionally present)
2	Ce(NO ₃) ₃	1	8-9	Flower-like microspheres around 10 μm in diameter assembled from microrods (ribbon-like microstructures additionally present)
3	Ce(OAc) ₃	0	8-9	Passion flower-like microstructures 30 – 50 μm in size
4	Ce(OAc) ₃	1	8-9	Microsized spheres assembled from irregular nanorods with rough edges
5	Ce(NO ₃) ₃	0	7	Irregular microsized assemblies of nanosheets
6	Ce(NO ₃) ₃	1	7	Flower-like structures up to 10 μm in size built from nanosheets

The crystal structure of Ce₂(WO₄)₃ was first reported by Gressling et al. in 1995.¹⁷ The compound shows monoclinic symmetry with a *C2/c* space group, where *a* = 7.813(4) Å, *b* = 11.720(2) Å, *c* = 11.586(3) Å, β = 109.36(3) °, and *Z* = 4. The crystal structure of Ce₂(WO₄)₃ is shown in Fig. 1. As can be seen from the structure there is only one Ce³⁺ lattice site, where the Ce³⁺ ion is coordinated by eight O²⁻ ions. W atoms are found in WO₄ tetrahedra and square WO₅ pyramids. Besides the Ce₂(WO₄)₃ compound also a crystal structure of Ce₁₀W₂₂O₈₁ can be found in the Inorganic Crystal Structure Database (ICSD).¹⁸ The Ce₁₀W₂₂O₈₁ compound shows orthorhombic symmetry with a *Pbnm* space group, where *a* = 3.8891(4) Å, *b* = 36.080(4) Å, *c* = 21.901(2) Å, β = 90 ° and *Z* = 2. As can be seen from the crystal structure (also Fig. 1) there are three non-equivalent Ce³⁺ lattice sites (each represented in a different color). One of these lattice sites is seven-coordinated, one is eight-coordinated, and one nine-coordinated by O²⁻ ions. W atoms are found in WO₅ pyramids, and also in WO₆ and WO₇ polyhedra, which share edges and corners to form W₆O₁₇ units.

The reaction parameters, corresponding morphologies and symbols, which have been assigned to the samples, are summarized in Table 1.

To analyze the material first the XRD patterns of 1-6 precursor samples (as prepared, before heat treatment) were recorded, yet they could not be matched with any standard XRD patterns found in the JCPDS database. Other reported rare-earth tungstate precursor materials synthesized in the presence of surfactants could not be matched with known XRD patterns either.¹⁹⁻²⁰ Fig. 2

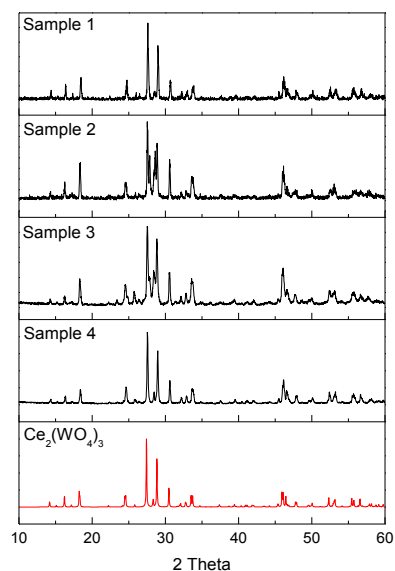


Fig. 2 XRD patterns of samples 1-4. A standard pattern of Ce₂(WO₄)₃ is shown in red.

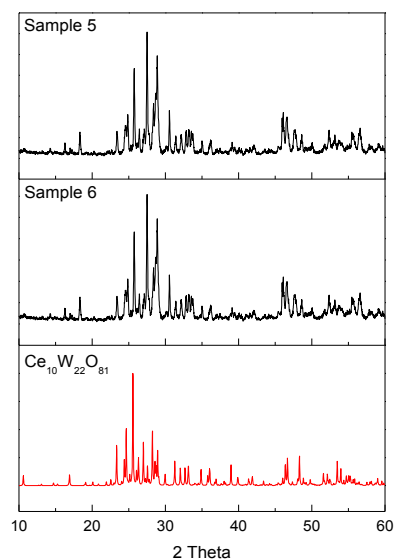


Fig. 3 XRD patterns of samples 5-6. A standard pattern of Ce₁₀W₂₂O₈₁ is shown in red.

shows XRD patterns of the samples 1-4 after heat treatment at 900 °C for 3h. As can be seen they can be matched to the pure monoclinic Ce₂(WO₄)₃ phase. Fig. 3 presents XRD patterns of the samples 5-6 after heat treatment at 900 °C for 3h. These samples can be matched with the pure orthorhombic Ce₁₀W₂₂O₈₁ phase. In all cases the presence of the DSS surfactant did not influence the formed phase. As can be seen changing the reaction pH from 8-9 to neutral pH, as well as the RE : W ratio, changed the phase from Ce₂(WO₄)₃ to Ce₁₀W₂₂O₈₁. Yet, this was only true for the reactions where Ce(NO₃)₃ was used as the source of Ce³⁺ ions. When Ce(OAc)₃ was employed in the reaction, and the pH was

adjusted to 7, the XRD patterns could not be matched to any known pure phase. The samples were further analyzed through DRIFTS infrared spectroscopy. (DRIFTS spectra of sample 1-6 are presented in Fig. S1). In sample 1 as no vibrations attributed to the O-H stretch vibrations are present in the spectra one can assume that after heat treatment all of the water molecules present on the surface of the material have been removed. Also no organic bands, which could be attributed to the presence of the DSS surfactant, can be detected in samples 2 and 4. Therefore it can be concluded that the surfactant is also completely burned off during the heat treatment process. In all the samples below 1000 cm^{-1} the characteristic tungstate vibrations are visible. For example for sample 1 the bands at 955 cm^{-1} and 884 cm^{-1} are attributed to the W-O stretch vibrations, and the band at 746 cm^{-1} is attributed to the asymmetric stretch vibrations of W-O-W bridges.²¹ Similar peaks (sometimes with slightly shifted wavenumbers) are observed for samples 2-4. In both sample 5 and 6 at around $1622\text{-}1633\text{ cm}^{-1}$ there is a small peak, which can be assigned to the O-H stretch vibrations. This means that some small amounts of water may be present on the surface of these materials. No organic bands, which could be assigned to the DSS surfactant are present in sample 6. The samples also show the characteristic W-O and W-O-W bands below 1000 cm^{-1} .

The morphology of samples 1-6 was characterized by SEM. Fig. 4 presents the morphology of the cerium tungstate samples obtained from $\text{Ce}(\text{NO}_3)_3$, at pH = 8-9, both in the presence and absence of DSS (samples 1 and 2). When no DSS was used (sample 1, Fig. 4a,b) irregular flower-like microspheres around 2–3 μm in diameter were formed. These flower-like microstructures were built from nanosized rods assembled together. Additionally nanosized spherical particles were sometimes present on the surface of the microstructures. When DSS was used in the reaction flower-like microspheres around 10 μm in diameter, assembled from microrods were obtained (sample 2, Fig. 4c,d). In this case besides the flower-like microstructures also ribbon-like microstructures could be found.

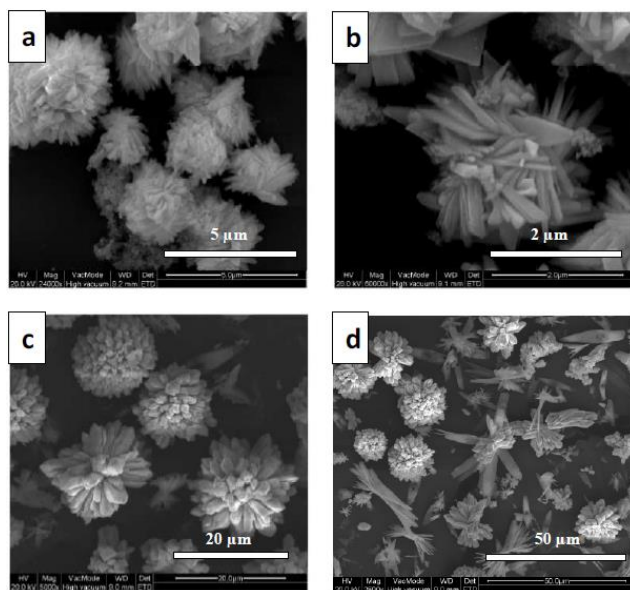


Fig. 4 SEM images at different magnifications of samples 1 (a-b) and 2 (c-d).

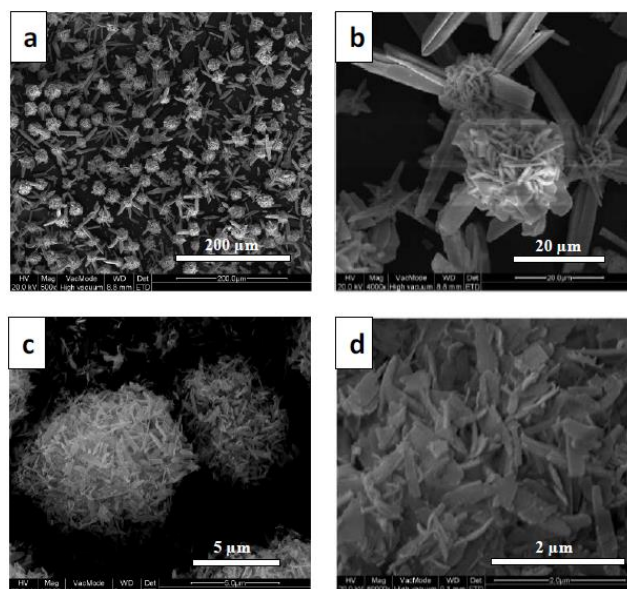


Fig. 5 SEM images at different magnifications of samples 3 (a-b) and 4 (c-d).

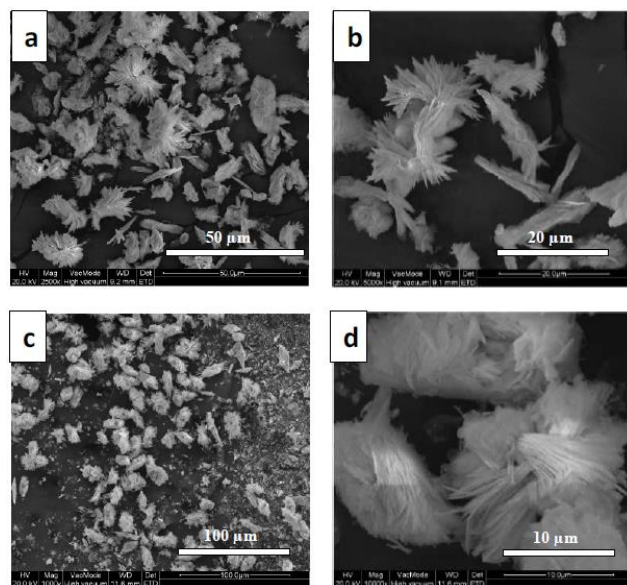


Fig. 6 SEM images at different magnifications of samples 5 (a-b) and 6 (c-d).

It can be concluded that when $\text{Ce}(\text{NO}_3)_3$ was used in the synthesis, although a pure phased material was obtained, the material did not show completely uniform morphology. Fig. 5 presents the morphology of the cerium tungstate samples obtained from $\text{Ce}(\text{OAc})_3$, at pH = 8-9, both in the presence and absence of DSS. As can be seen in Fig. 5a,b when no DSS is present in the reaction microstructures, which can be best compared to passion flowers, were formed (sample 3). These structures were quite large – usually between 20-50 μm . When DSS was used in the reaction microspheres, usually around 5 μm in size were formed. They are built from irregular nanorods with rough edges (sample 4, Fig. 5c,d). The nanorods are packed very tightly together to form the microstructures. When the pH of the reaction was changed to 7 samples 5 and 6 were formed. Their morphology is presented in Fig. 6. When no DSS was present in

the reaction medium during the synthesis irregular structures built from nanosheets were obtained (sample 5, Fig.6a,b). Depending on the packing of the nanosheet building blocks some of them form bowknot-like structures. When DSS was additionally used flower-like structures up to 10 μm in size were formed (sample 6, Fig. 6c,d). These microstructures are built by multiple nanosheets layered on top of each other. As previously mentioned when $\text{Ce}(\text{OAc})_3$ was employed in the reaction and the pH adjusted to 7, the XRD patterns could not be matched to any known pure phase. Because of this the morphology of these materials was not studied.

Luminescence properties

In this study we have synthesized two types of cerium tungstate materials and we have studied their luminescence properties after doping them with trivalent terbium ions. Terbium ions were chosen among the lanthanides, as it is known that an efficient energy transfer can occur between the Ce^{3+} and Tb^{3+} ions. Several articles can be found where Tb^{3+} ions are doped into a cerium material (for example CeO_2) or where a Tb^{3+} doped material is additionally co-doped with Ce^{3+} ions to enhance the luminescence. In this research our goal was to study the luminescence properties of $\text{Tb}:\text{Ce}_2(\text{WO}_4)_3$ and $\text{Tb}:\text{Ce}_{10}\text{W}_{22}\text{O}_{81}$ with different morphologies, but also to understand the energy transfer mechanism in this tungstate-cerium-terbium system.

Fig. 7 presents the room-temperature combined excitation - emission spectrum of **5% Tb doped 1**, after annealing at 900 $^\circ\text{C}$ (all samples were doped with 5% Tb). The excitation spectrum contains a strong and broad band with a maximum at around 260.0 nm, which corresponds to the charge-transfer from the 2p orbitals of the oxygens to the 5d orbitals of the tungsten. No characteristic bands of the Tb^{3+} or broad band of Ce^{3+} can be detected in the excitation spectrum. The emission spectrum contains four sharp emission peaks characteristic of Tb^{3+} ions. Peak a can be assigned to the $^5\text{D}_4 \rightarrow ^7\text{F}_6$ transition, peak b to the $^5\text{D}_4 \rightarrow ^7\text{F}_5$ transition, peak c to the $^5\text{D}_4 \rightarrow ^7\text{F}_4$ transition, and peak d to the $^5\text{D}_4 \rightarrow ^7\text{F}_3$ transition. The wavelength and wavenumber values of the peaks are given in Table 2. No broad emission peaks, which could be appointed either to the Ce^{3+} ions or the tungstate band, are visible in the spectrum. Fig. 8 compares the emission spectra of **5% Tb doped 1-4** when excited at 260.0 nm. In the emission spectra only the characteristic peaks of Tb^{3+} can be observed. The different intensities of the peaks in the excitation emission spectra, as well as slight peak shifts and some small changes in the peak splitting indicate different environment around the ions (which can be explained by different morphologies of the four $\text{Ce}_2(\text{WO}_4)_3$ materials as seen in Fig. 4 and Fig. 5). A change in luminescence intensity for materials with different morphologies has numerously been reported. In all cases a strong broad band, with a maximum around 260.0 nm is visible in the excitation spectra (Fig. S2). No other peaks are present in the excitation spectrum.

Fig. 9 presents the room-temperature combined excitation-emission spectrum of **5% Tb doped 6**. In the excitation spectrum two broad bands are present, one with a maximum at around 260.0 nm and the other at around 366.0 nm. The first one can be assigned to the W-O charge transfer band, while the other is assigned to be Ce^{3+} band. When excited into the W-O band the

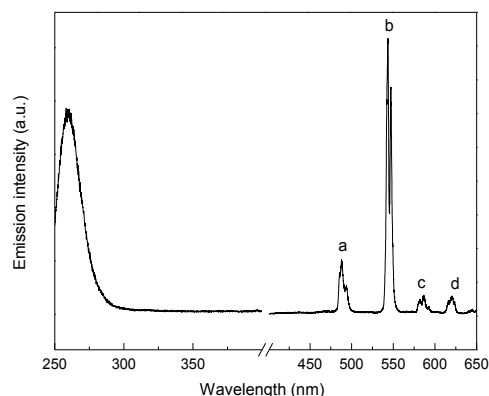


Fig. 7 Excitation spectrum (monitored at 543.6 nm) and emission spectrum (excited at 260.0 nm) of **5% Tb doped 1**. The electronic transitions labeled a-d are assigned in Table 2.

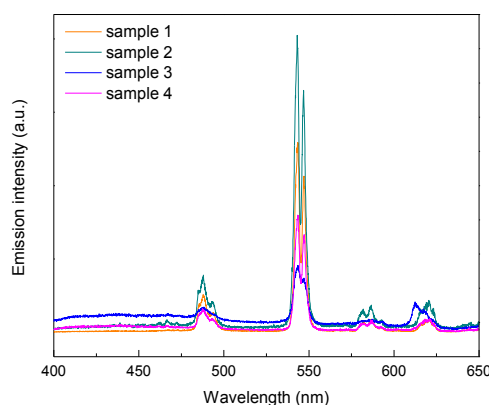


Fig. 8 Emission spectra of **5% Tb doped 1, 2, 3, and 4** when excited at 260.0 nm.

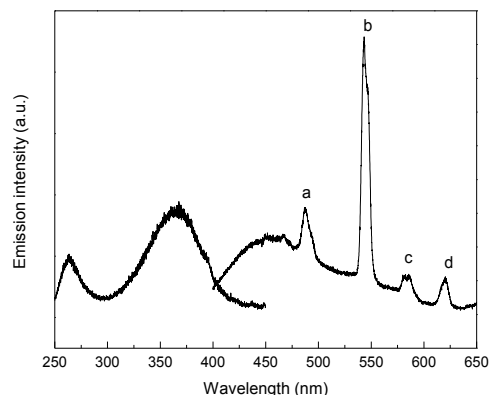


Fig. 9 Excitation spectrum (monitored at 543.4 nm) and emission spectrum (excited at 270.0 nm) of **5% Tb doped 6**. The electronic transitions labeled a-d are assigned in Table 2.

material shows all of the characteristic peaks of Tb^{3+} , which unlike in the spectra of the $\text{Tb}:\text{Ce}_2(\text{WO}_4)_3$ embedded on a

broad band ranging from around 400.0–550.0 nm. This broad band can be assigned to the 5d-transitions of Ce^{3+} between the $^2\text{F}_{5/2}$ ($4f_1$) ground state and the ^2D ($5d_1$) state, as well as the W-O band. Fig. 10 compares the emission spectra of **5% Tb doped 1** and **5% Tb doped 6** with rainbow curves underneath to show the different color components, as well as the CIE color diagrams with the x and y coordinates of the two samples marked on the diagrams.

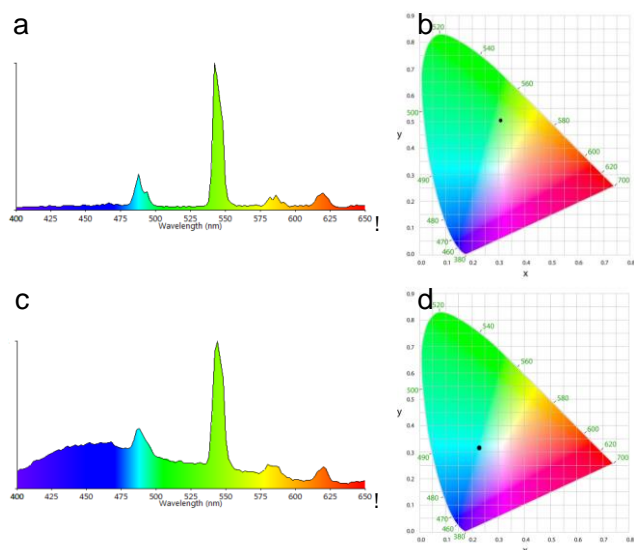


Fig. 10 Top left: emission spectrum of **5% Tb doped 1** (excited at 260.0 nm) with rainbow plotted under curve to show the different color components. Top right: CIE color diagram; the black dot shows the x and y color coordinates of the sample ($x = 0.31$, $y = 0.51$). Bottom left: emission spectrum of **5% Tb doped 6** (excited at 270.0 nm) with rainbow plotted under curve to show the different color components. Bottom right: CIE color diagram; the black dot shows the x and y color coordinates of the sample ($x = 0.23$, $y = 0.32$).

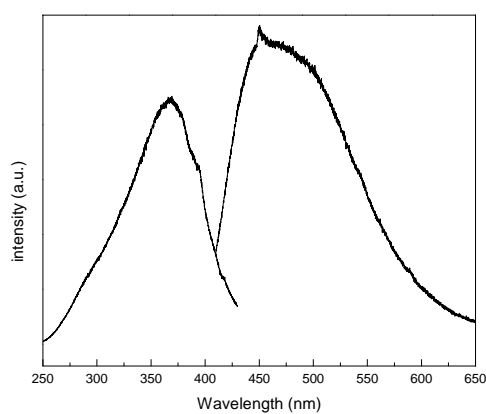


Fig. 11 Excitation spectrum (monitored at 430.0 nm) and emission spectrum (excited at 366.0 nm) of **5% Tb doped 6**.

Table 2. Assignment of labeled transitions shown in Fig. 7 and Fig. 9.

Label	Transition	5% Tb doped 1		5% Tb doped 6	
		nm	cm^{-1}	nm	cm^{-1}
a	$^5\text{D}_4 \rightarrow ^7\text{F}_6$	488.3	20479	486.7	20547
b	$^5\text{D}_4 \rightarrow ^7\text{F}_5$	543.6	18396	543.4	18403
c	$^5\text{D}_4 \rightarrow ^7\text{F}_4$	586.9	17039	585.9	17068
d	$^5\text{D}_4 \rightarrow ^7\text{F}_3$	620.4	16119	620.3	16121

On the other hand when the **5% Tb doped 6** material is excited at 366.0 nm (into the Ce^{3+} band) only a strong, broad band is observed in the emission spectrum (Fig. 11). The band has a maximum at around 460.0 nm. No peaks of terbium are present in the emission spectrum. The combined excitation - emission spectrum of **5% Tb doped 5** is presented in Fig. S3. In the excitation spectrum of this sample mostly a broad band, which can be assigned to the tungstate charge-transfer band is visible. A weak band in the region that a band from Ce^{3+} would be expected is also visible. Similarly to **5% Tb doped 6** exciting the sample into the two bands yields different emission spectra. Table S1 gathers the CIE color coordinates of **5% Tb doped 1-6**. The energy transfer mechanisms for the two different Tb doped cerium tungstate materials have been proposed in Fig. 12 and Fig. 13. For the **5% Tb doped 1** sample the excitation of the O-W ligand-to-metal charge transfer band of the $\text{Ce}_2(\text{WO}_4)_3$ material causes population of the terbium $^5\text{D}_3$ excited state. The following mechanism is suggested: the sample is excited at 266.0 nm into the tungstate charge transfer band. From the excited W-O charge transfer electronic state the energy is passed on to the acceptor energy state of Tb^{3+} , from which it decays nonradiatively to the $^5\text{D}_4$ state followed by radiative decay to the lower levels of $^7\text{F}_j$ ($J = 0-6$). Due to this characteristic emission peaks of Tb^{3+} are observed. The **5% Tb doped 6** sample can be excited both into the W-O charge transfer band (at 270.0 nm) or into the Ce^{3+} band (at 366.0 nm). When excited at 270.0 nm, into the tungstate charge transfer band (marked as process 1), energy can be transferred from the excited charge-transfer electronic state on to the acceptor energy state of Tb^{3+} , from which it decays nonradiatively to the $^5\text{D}_4$ state followed by radiative decay to the lower levels of $^7\text{F}_j$ ($J = 0-6$). This gives rise to the characteristic peaks of Tb^{3+} . Also energy from the excited charge-transfer electronic state can be transferred to the ^5D state of Ce^{3+} and its emission can be seen as a broad band in the region of 400.0-500.0 nm. Additionally energy from the excited charge transfer state can be relaxed back to the W-O ground state yielding a broad band in the 400-550 nm region. The **5% Tb doped 6** sample can also be excited into the 366.0 nm transition band of Ce^{3+} (marked as process 2). In this case energy is transferred from the $^5\text{D}_{5/2}$

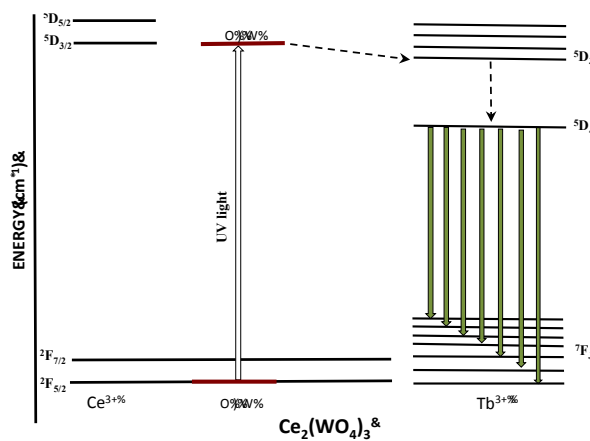


Fig. 12 Energy transfer diagram in **5% Tb doped 1** sample.

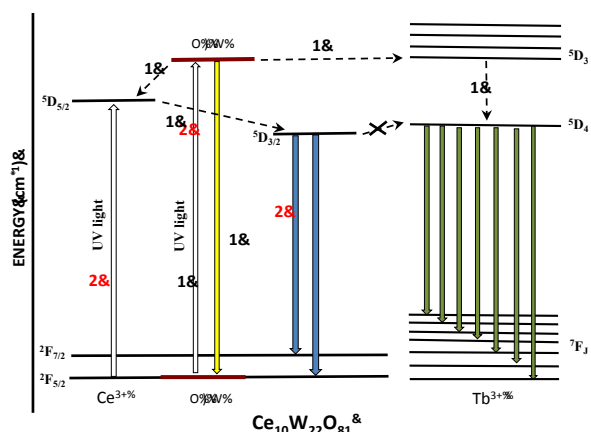


Fig. 13 Energy transfer diagram in 5% Tb doped 6 sample.

state to the $^5D_{3/2}$ state of Ce^{3+} , yet it can not be further transferred to the acceptor energy states of Tb^{3+} (the acceptor states are located at higher energy than the $^5D_{3/2}$ state of cerium). Therefore in this case only a broad emission peak located in the 400.0-600.0 nm region is observed in the emission spectrum.

Conclusions

In summary, we have successfully synthesized two cerium tungstate materials ($Ce_2(WO_4)_3$ and $Ce_{10}W_{22}O_{81}$) with micro-sized 3D architectures. A simple hydrothermal synthesis was employed to obtain the precursor materials. After heat treatment at 900 °C, the precursors were transformed into the desired materials. We have studied the influence of the lanthanide source and DSS surfactant on the size and morphology of these materials. This study showed that the presence of DSS significantly changed the shape of the building blocks, and consequently the final architecture of the microstructure. We also established that the source of the cerium ions (nitrate or acetate salt) plays an important role in the size and shape formation. The luminescence properties of these materials were investigated. Depending on the morphology the materials showed some changes in the luminescence spectra. Different energy transfer mechanisms were proposed for the two cerium tungstate materials. The CIE color coordinates of the materials were calculated. It was observed that the 5% Tb: $Ce_2(WO_4)_3$ microstructures emitted green light, whereas the 5% Tb: $Ce_{10}W_{22}O_{81}$ microstructures emitted either blue or green light depending on the excitation wavelength.

Acknowledgments

RVD thanks the Hercules Foundation (project AUGÉ/09/024 "Advanced Luminescence Setup"), and Ghent University (UGent; project BOF 01N01010) for funding. KVH thanks the Hercules Foundation (project AUGÉ/11/029 "3D-SPACE: 3D Structural Platform Aiming for Chemical Excellence") and the Research Fund – Flanders (FWO) for funding.

Notes and references

^a L^3 - Luminescent Lanthanide Lab, Department of Inorganic and Physical Chemistry, Ghent University, Krijgslaan 281-S3, B-9000 Ghent, Belgium
E-mail: rik.vandeun@ugent.be

^b E-mail: anna.kaczmarek@ugent.be

^b XStruct, Department of Inorganic and Physical Chemistry Ghent University, Krijgslaan 281-S3, B-9000 Ghent, Belgium
^c SCRiPTS, Department of Inorganic and Physical Chemistry Ghent University, Krijgslaan 281-S3, B-9000 Ghent, Belgium

† Electronic Supplementary Information (ESI) available: DRIFTS spectra of samples 2, 3, 4, 5; excitation spectra of 5% Tb doped 2, 3, 4; combined excitation-emission spectrum of 5% Tb doped 5; table with CIE color coordinates of 5% Tb doped 1-6 See DOI: 10.1039/b000000x/

- H. Colfen and S. Mann, *Angew. Chem., Int. Ed.*, 2003, **42**, 2350.
- M. Li, H. Schnablegger and S. Mann, *Nature*, 1999, **402**, 393.
- G. Liu, X. Chen, Handbook on the Physics and Chemistry of Rare Earths, Gschneidner, K.A. Jr.; Bünzli, J.-C.G.; Pecharsky, V. K. Elsevier Science: Amsterdam, 2007; Vol. 37, Chapter 233, pp. 99–169.
- R. N. Bhargava, *J. Lumin.*, 1996, **70**, 85.
- B. M. Tissue, *Chem. Mater.*, 1998, **10**, 2837.
- T. Jüstel, J.-C. Krupa, D. U. Wiechert, *J. Lumin.*, 2001, **93**, 179.
- Z. Hou, Z. Cheng, G. Li, W. Wang, C. Peng, C. Li, P. Ma, D. Yang, X. Kang, J. Lin, *Nanoscale*, 2011, **3**, 1568.
- Y. Zheng, H. You, K. Liu, Y. Song, G. Jia, Y. Huang, M. Yang, L. Zhang, G. Ning, *CrystEngComm*, 2011, **13**, 3001.
- J. Wang, Z.-J. Zhang, J.-T. Zhao, H.-H. Chen, X.-X. Yang, Y. Tao, Y. Huang, *J. Mater. Chem.*, 2010, **20**, 10894.
- A. M. Kaczmarek, R. Van Deun, *Chem. Soc. Rev.*, 2013, **42**, 8835.
- A. M. Kaczmarek, K. Van Hecke, R. Van Deun, *Inorg. Chem.*, 2014, **53**, 9498.
- Y. Zheng, Z. Li, L. Wang, Y. Xiong, *CrystEngComm*, 2012, **14**, 7043.
- L. Xu, J. Shen, C. Lu, Y. Chen, W. Hou, *Cryst. Growth Des.*, 2009, **9**, 3129.
- L. Xu, X. Yang, Z. Zhai, D. Gu, H. Pang, W. Hou, *CrystEngComm*, 2012, **14**, 7330.
- Y. Zhou, B. Yan, X.-H. He, *J. Mater. Chem. C* 2014, **2**, 848.
- S. Pramanik, S. C. Bhattacharya, *Mater. Chem. Phys.*, 2010, **121**, 125.
- T. Gressling, Hk. Müller-Buschbaum *Z. Naturforschung*, 1995, **50b**, 1513.
- R. S. Barker, I. R. Evans, *Acta Cryst.*, 2008, **B64**, 708.
- A. M. Kaczmarek, Y.-Y. Liu, P. Van Der Voort, R. Van Deun, *Dalton Trans.*, 2013, **42**, 5471.
- S. Huang, X. Zhang, L. Wang, L. Bai, J. Xu, C. Li, P. Yang, *Dalton Trans.*, 2012, **41**, 5634.
- F. Lei, B. Yan, *J. Mater. Res.*, 2011, **26**, 88.
- P. Ghosh, A. Kar, A. Patra, *Nanoscale*, 2010, **2**, 1196.
- H. A. A. Seed Ahmed, O. M. Ntwaeaborwa, R. E. Kroon, *Curr. Appl. Phys.*, 2013, **13**, 1264.
- V. Pankratov, A. I. Popov, S. A. Chernov, A. Zharkouskaya, C. Feldmann, *Phys. Status Solidi B*, 2010, **247**, 2252.
- F. T. Rabouw, S. A. den Hartog, T. Senden, A. Meijerink, *Nature Comm.*, 2014, doi:10.1038/ncomms4610.
- X. Wang, D. Zhang, Y. Li, D. Tang, Y. Xiao, Y. Liu, Q. Huo, *RSC Adv.*, 2013, **3**, 3623.
- J. Sokolnicki, *J. Lumin.*, 2013, **134**, 600.
- H. Jiao, N. Zhang, X. Jing, D. Jiao, *Opt. Mater.*, 2007, **29**, 1023.
- D. Chen, G. Shen, K. Tang, Z. Liang, H. Zheng, *J. Phys. Chem. B*, 2004, **108**, 11280.
- W. Chen, A. G. Joly, C. M. Kowalchuk, J.-O. Malm, Y. Huang, J.-O. Bovin, *J. Phys. Chem. B*, 2002, **106**, 7034.
- G. Li, C. Peng, C. Zhang, Z. Xu, M. Shang, D. Zhang, X. Kang, W. Wang, C. Li, Z. Cheng, J. Lin, *Inorg. Chem.*, 2010, **49**, 10522.
- J. Liu, B. Xu, C. Song, H. Luo, X. Zuo, L. Han, X. Yu, *CrystEngComm*, 2012, **14**, 2936.